IEEE Photonics Journal
An IEEE Photonics Society Publication

Open Access

Cascaded Graphene Frequency Selective Surface Integrated Tunable Broadband Terahertz Metamaterial Absorber

Volume 11, Number 2, April 2019

Rishi Mishra
Arpit Sahu
Ravi Panwar, ***Member, IEEE***

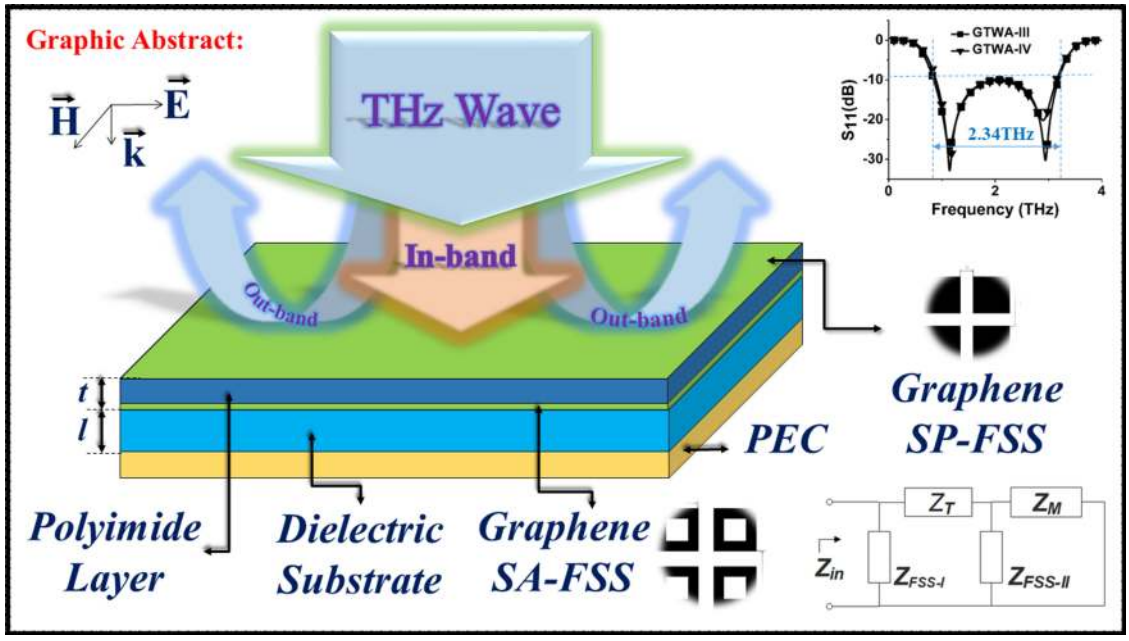

DOI: 10.1109/JPHOT.2019.2900402

Cascaded Graphene Frequency Selective Surface Integrated Tunable Broadband Terahertz Metamaterial Absorber

Rishi Mishra, Arpit Sahu, and Ravi Panwar, *Member, IEEE*

Discipline of Electronics and Communication Engineering, Indian Institute of Information Technology, Design and Manufacturing, Jabalpur, Jabalpur 482005, India

DOI:10.1109/JPHOT.2019.2900402

Manuscript received January 21, 2019; revised February 13, 2019; accepted February 14, 2019. Date of publication March 5, 2019; date of current version March 19, 2019. This work was supported by the Science and Engineering Research Board (SERB), Department of Science and Technology (DST), Government of India under Early Career Research Grant (ECR/2017/000676) and Faculty Initiation Grant, Indian Institute of Information Technology, Design and Manufacturing Jabalpur, Madhya Pradesh, India. Corresponding author: Ravi Panwar (e-mail: rpanwar.iitr@gmail.com).

Abstract: The quest of novel materials and structures to design an efficient absorber for realizing wave trapping and absorption at terahertz (THz) frequencies is an open topic. But the design of a thin, wideband, and tunable THz absorber is still an arduous job. Hence, in this paper, a hybrid THz metamaterial absorber integrated with a cascaded graphene frequency selective surface (FSS), with ultra-high absorbance over a wide frequency range is designed using an analytical equivalent circuit model. Such an approach provides a feasible way to optimize the device by interrelating the effective electromagnetic and circuit parameters with the unit cell dimensions of FSS. A systematic study and critical analysis over a wide range of device parameters including graphene chemical potential and FSS design variables is demonstrated. A peak dip in reflection coefficient of −30.27 dB is observed at 2.94 THz for an optimal device with a chemical potential (μ_c) of 0.38 eV (μ_{c1}), and 0.25 eV (μ_{c2}) in the range of 0.1–4.0 THz. The cascaded FSS configuration results in the unique anti-reflection-based absorption phenomena, which is responsible for the achievement of –10 dB absorption bandwidth of 2.34 THz (0.85–3.19 THz). In addition, the frequency-dependent effective permittivity, permeability, and impedance is extracted using reflection data, in order to understand the device physics. Such ultra-thin and broadband absorbing device architecture may confer potential application perspectives in THz sensing, imaging, and detection.

Index Terms: Metamaterial, engineered photonic structure, frequency selective surface, terahertz sensing, equivalent circuit model.

1. Introduction

Terahertz (THz) technology has emerged as a vital field to discover the possibilities of the future generation technologies. Several new research areas have been developed after exploration of its potential applications such as earth sensing, astronomy, medical sensing and imaging, biotech, spectroscopy, defense, security, industrial, remote sensing, and wireless communications, etc. [1]–[4]. Many sensing and measuring devices are existing to detect microwave radiation, but they hindered progress at THz frequency. The upgradation of these devices or the development of new devices is very much required in order to realize such potential applications. Hence, THz absorbers are to be essentially explored to fulfil such requirements [1]. But the development of

thin and broadband THz absorber with tunable absorption properties is a very difficult job for the researchers.

Recently, metamaterials (MMs) have become an emerging research topic, due to its exotic properties [5], [6]. Many devices have been synthesized based on the analysis of these properties, and effects [7]–[9]. Metamaterial absorber (MMA) can make nearly perfect absorption at the resonating frequencies. In 2008, Landy *et al.* [10] has presented the first MMA comprising of a sandwich structure of a metallic cut wire, a dielectric substrate, and a split ring resonator. After that, many efforts have been made by the researchers to enhance the properties for other regions [11]–[14] including mm wave frequency band [13], and infrared bands [14]. Gasmelseed *et al.* [15] have reported the effect of MMs in order to achieve superior microwave absorption properties.

Graphene can be a good material for THz application as it has some unique chemical and electrical properties, which have rarely found in other nanomaterials [16]–[21]. Graphene contains intra-band conductivity and inter-band conductivity, which can be controlled by electrostatic or magnetic field [18], [19]. Various devices have been designed for THz-wave absorption after analyzing these frequency dependent conductivities of the graphene [20], [21]. However, the only graphene sheet has been considered, while designing these devices. Very few devices have been designed, based on the metamaterial and graphene frequency selective surface (GFSS) integrated structures. FSSs are the periodically oriented advanced electromagnetic (EM) structures; acting as an EM-wave filter [22], [23]. Due to its potential frequency filtering properties, these structures are considered for the antenna radomes, stealth structures, radar cross section (RCS) reduction, and metamaterials, etc. [23], [24]. Nowadays, enough motivation has been observed to explore the FSSs in THz absorption. A number of structures have been designed to make wideband, and tunable absorbers [25], [26]. Graphene FSS can make a remarkable enhancement in absorption bandwidth, while designing a tunable THz absorber.

Design of graphene absorbers with high accuracy is difficult and also very expensive because of its costly laboratory equipment. Hence, multiple interference theorems, and transfer matrix were proposed in [18], [26], [27] to analyze; they are unable to provide a proper guidance on the development of a reliable and accurate graphene absorbers. Numerical methods such as the frequency domain time difference (FDTD), periodic method of moments (PMM), finite element method (FEM) etc., may give excellent precision, however, these techniques are time consuming, and requires high performance computational facilities. Hence, in the development of the graphene absorbers, ECM can be considered as an efficient tool [21], [22]. The basic physics behind the absorption can be explained by ECM as it provides typical analytical values of basic electric parameters (i.e., resistance, capacitance, and inductance) of the device, which reduces the efforts in designing of the absorbers and makes the analysis more effective and accurate.

Sufficient amount of researches has been carried out by scientists and researchers in order to design the MM based THz absorbers [13], [26]. In [28], Ye *et al.*, has presented wide absorption angle characteristic of MMA. Pan *et al.* [29], has illustrated the mechanism that provides the complete analysis of MM absorption. The research summarizes that the larger absorption have been carried out by EM. Wilbert *et al.* have demonstrated the experimental and simulation results of a polarization angle-insensitive fourfold symmetric terahertz MMA [30]. A great effort has been made by Hunag *et al.* [31] in the development of graphene patch array based THz wave absorber using ECM. The effective absorption bandwidth of 1.46 THz has been noticed over 90% absorption. Based on their work, we have initiated a study to examine the effect of single and Double Square FSSs made of copper, instead of graphene over the absorption characteristics of THz absorber. The absorption characteristics have been found to be improved with the application of aperture geometries.

In the quest of thin and broadband absorber, there is still a probability to further improvement of the absorption properties by employing the concept of multi-layering and cascading graphene FSSs. In this article, a hybrid and tunable multilayered THz-MMA integrating with cascaded graphene FSSs and dielectric layers is designed at THz frequencies using an efficient ECM approach. Such a THz wave absorbing configuration is superior as compared to the existing single-layers

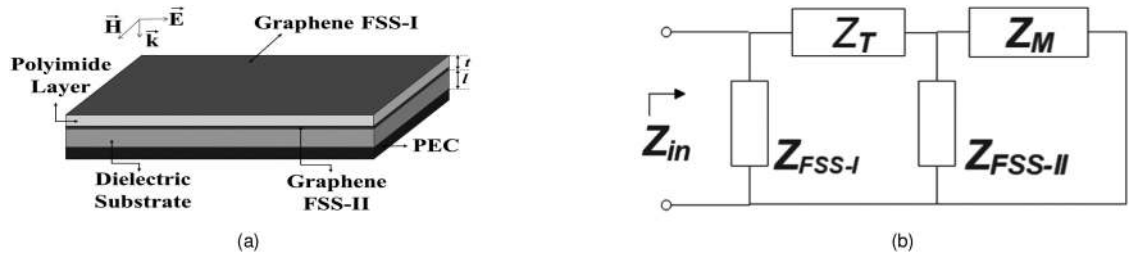

Fig. 1. Proposed five layered THz-MMA (a) Schematic device structure, and (b) TLM.

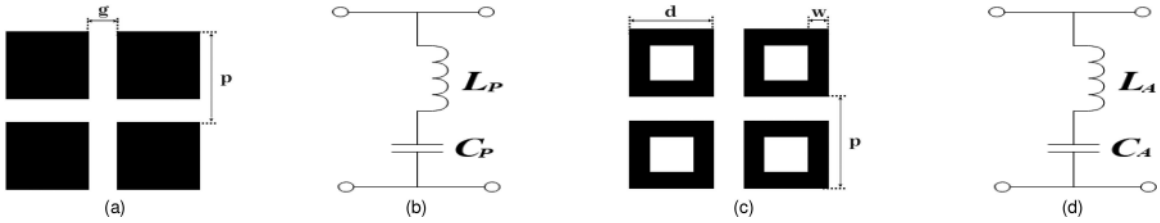

Fig. 2. Proposed FSS geometries and corresponding ECs (a) SP-FSS (b) EC of SP-FSS (c) SA-FSS, and (d) EC of SA-FSS.

TABLE 1
Different THz Wave Absorber Configurations

THz wave absorber configuration	Symbol
Graphene Patch/Polyimide layer/Graphene sheet	GTWA-I
Graphene Aperture/Polyimide layer/Graphene sheet	GTWA-II
Top patch FSS/Polyimide layer/Bottom aperture FSS	GTWA-III
Top aperture FSS/Polyimide layer/Bottom patch FSS	GTWA-IV

THz-MMAs in terms of lower thickness, −10 dB absorption bandwidth, and comparable absorption efficiency.

2. Theoretical Background and Design Methodology

In this work, a five layer hybrid THz-MMA structure has been proposed as shown in Fig. 1(a) along with a corresponding transmission line model (TLM) as depicted in Fig. 1(b). Here, graphene monolayer based FSSs, separated by a thin layer of polyimide, were embedded into the dielectric substrate (relative permittivity ϵ_{rl} of 5) backed with a ground plane. Two types of graphene monolayer FSS, i.e., graphene square patch array, and graphene square aperture array, have been considered for the design of a tunable THz-MMA. The schematic diagrams of proposed FSSs with corresponding equivalent circuit (EC) diagrams are presented in Figs. 2(a)–(d), respectively. The design variables for square patch FSS (SP-FSS) are 'g', and 'P'. Here, 'g' is the gap between the square patches, and 'P' is the periodicity of the SP-FSS unit cell.

In the same way, the design variables for square aperture FSS (SA-FSS) are 'p', 'd', and 'w'. Here, 'p' represents the periodicity of the unit cell, 'w' is the width of strip, and 'd' is the length of a single square. The gap between two square aperture 'g_a' = p–d. The inductance (L) and capacitance (C) of the patch and apertures geometries is represented by (L_P, C_P) and (L_A, C_A), respectively. Table 1 presents the details of distinct THz-MMA configurations (i.e., GTWA- I, GTWA-II, GTWA-III, and GTWA-IV) proposed for the current study. The first configuration GTWA-I comprises of a graphene patch array and a continuous graphite sheet, separated by a thin polyimide layer, as

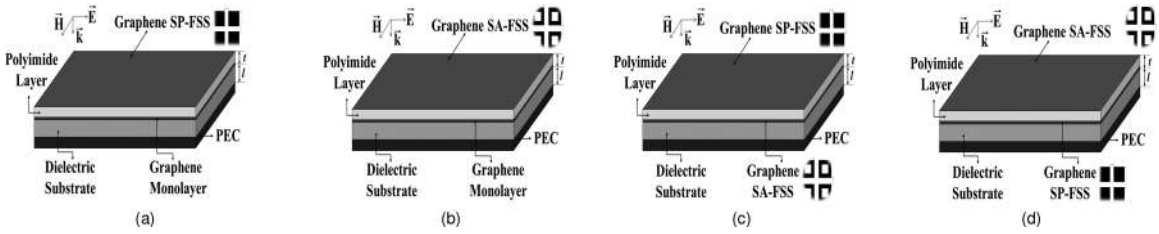

Fig. 3. Schematics of proposed THz-MMA configurations. (a) GTWA-I (b) GTWA-II (c) GTWA-III (d) GTWA-IV.

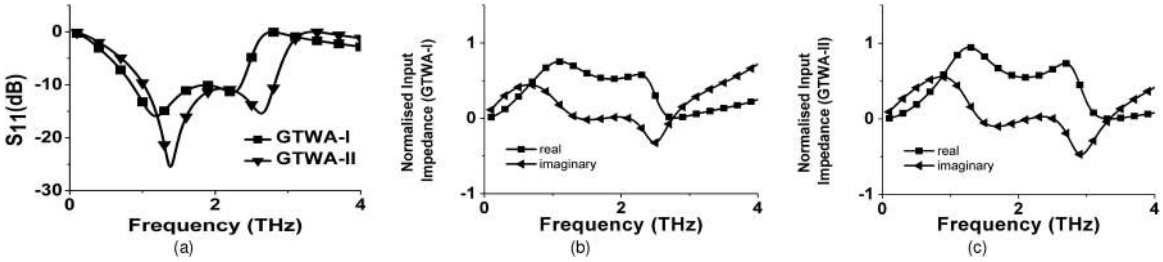

Fig. 4. Frequency dependent characteristics of THz-MMA configurations GTWA-I and GTWA-II. (a) RC-frequency spectra's. (b) Normalized input impedance of GTWA-I. (c) Normalized input impedance of GTWA-II.

shown in Fig. 3(a). The graphene aperture array and continuous graphene sheet, separated by a thin polyimide layer, have been utilized for the design of the second configuration (i.e., GTWA-II), as depicted in Fig. 3(b). Further, two hybrid THz-MMA configurations (i.e., GTWA-III and GTWA-IV) integrated with cascaded FSS geometries have been introduced, which comprises of both kinds of FSS, i.e., graphene SP-FSS, and graphene SA-FSS with alternating positions, as shown in Figs. 3(c) and (d). In Fig. 3(c), FSS-I is graphene patch array (i.e., SP-FSS), and FSS-II is a graphene aperture array (SA-FSS), and vice-versa in Fig. 3(d).

The frequency-dependent complex surface conductivity of an isolated graphene sheet (typical thickness 0.34 nm) can be estimated as the sum of intra-band, and the inter-band conductivities [18]. The complex surface conductivity of graphene sheet can be given as [31]. The surface impedance of the graphene sheet (Z_G) can be given as [32]. The input impedance of the SP-FSS (Z_{GP}) can be described as [31]. The surface impedance of the SA-FSS can be calculated by:

$$Z_{GA} = \frac{p}{2w\sigma} + k\left(\omega L - \frac{1}{\omega C}\right) \cdot Z_c \tag{1}$$

where p is the period of the aperture array, w is the width of the aperture (as shown in Fig. 2), Z_c is the characteristic impedance, and ωL, ωC can be given as [22]. The impedance of a thin layer of polyimide (Z_T) and dielectric substrate (Z_M) can be calculated using [31]–[33]. The device impedance (Z_{in}) can be evaluated by solving the basic electrical circuit depicted in Fig. 1(b).

3. Results and Discussion

Fig. 4(a) depicts RC characteristics of two basic THz-MMA configurations (i.e., GTWA-I, and GTWA-II). The absorption bandwidth corresponding to −10 dB RC is achieved as 1.50 THz with a minimum RC value of −15.9 dB at 1.19 THz for GTWA-I. The real and imaginary parts of the normalized input impedance are shown in Fig. 4(b). One can see that the real values of the normalized input impedance tend to unity, when the imaginary part becomes zero at resonance frequencies. GTWA-II configuration with SA-FSS geometry provides a little bit larger absorption bandwidth than GTWA-I, as can be visualized in Fig. 4(a). It provides 1.79 THz absorption bandwidth with a

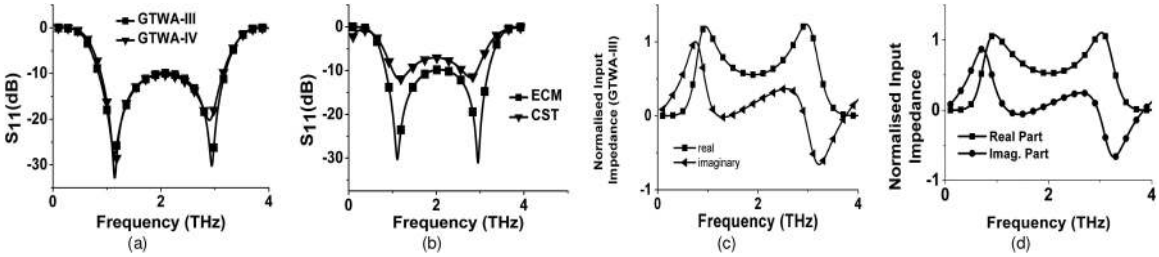

Fig. 5. RC characteristics with cascaded FSS geometries, i.e., GTWA-III and GTWA-IV. (a) RC-frequency spectra's. (b) Comparison of ECM and CST RC-frequency spectra's, (c) Normalized input impedance of GTWA-III. (d) Normalized input impedance of GTWA-IV.

TABLE 2
THz Wave Absorption Properties of Proposed Configurations

Symbol	Peak RC (dB)	Frequency of peak RC (THz)	-10 dB bandwidth (THz)
GTWA-I	-15.9	1.19	1.50 (0.85-2.35)
GTWA-II	-25.49	1.38	1.79 (1.02-2.81)
GTWA-III	-30.27	2.94	2.34 (0.85-3.19)
GTWA-IV	-32.83	1.14	2.26 (0.89-3.15)

minimum RC value of −25.49 dB at 1.38 THz. Fig. 4(c) shows the normalized input impedance of this configuration, which confirms the resonance at 1.38 THz, and 2.63 THz.

Further, an effort is made to improve the absorption characteristics by the application of hybrid THz-MMA configurations (i.e., GTWA-III, and GTWA-IV) comprising of cascaded graphene FSSs. GTWA- III configuration achieved a remarkable −10 dB absorption bandwidth of 2.34 THz (0.85–3.19 THz) with a minimum RC value of −30.27 dB at 2.94 THz as shown in Fig. 5(a). The spectra's of the normalized input-impedance of this configuration are depicted in Fig. 5(c). Similarly, a change in the position of FSS-I, and FSS-II has been made in the case of GTWA-IV configuration. SA-FSS is used as FSS-I, on the other hand, the SP-FSS is utilized as FSS-II. Since the input impedance of polyimide layer is very less than the FSS-impedance, the change should not affect much in total input impedance, and hence in the THz absorption. This can be verified by the results shown in Fig. 5(a), where −10 dB absorption bandwidth is observed as 2.26 THz (0.89–3.15 THz) with a peak RC value of −32.83 dB at 1.14 THz. The bandwidth consistent with this configuration is slightly lesser than the bandwidth achieved by GTWA-III, because of the impedance mismatch affected by polyimide layer as depicted in Figs. 5(c)–(d). The resonance frequencies of both the hybrid configurations (i.e., GTWA-III, and GTWA-IV) are same, i.e., 1.14 THz, and 2.94 THz, respectively, as shown in Fig. 5(a). Table 2 presents a systematic and critical analysis of THz absorption of adopted THz-MMA configurations, in terms of their peak RC values, S_{11} (dB), and −10 dB absorption bandwidth. It is clear that GTWA-III is the best THz-MMA configuration due to its broadband absorption (i.e., −10 dB absorption bandwidth of 2.34 THz) at THz regime. Moving one step further, RC characteristics of the optimal device extracted using ECM, are compared with those obtained using CST full wave simulations for the cross verification. A quite good agreement among ECM and CST data is observed with an approximately similar pattern, as clear from Fig. 5(b).

Graphene conductivity is highly dependent on its chemical potential (μ_c) [18]. Since, the THz absorption in GTWA-III is better than the other three THz-MMA configurations (i.e., GTWA-I, GTWA-II, and GTWA-IV), therefore, the effect of μ_c has been analyzed only for the optimal THz-MMA configuration, i.e., GTWA-III. Figs. 6(a) and (b) show the variation in RC characteristics by changing μ_c, μ_{c1} (ranging from 0.15 to 0.55 eV), while keeping μ_{c2} as 0.25 eV, and μ_{c2} (ranging from 0.18 to 0.58 eV), while keeping μ_{c1} as 0.38 eV, respectively. The first peak RC value is shifting towards the low frequency regime, whereas the second peak RC value is shifting towards high frequency

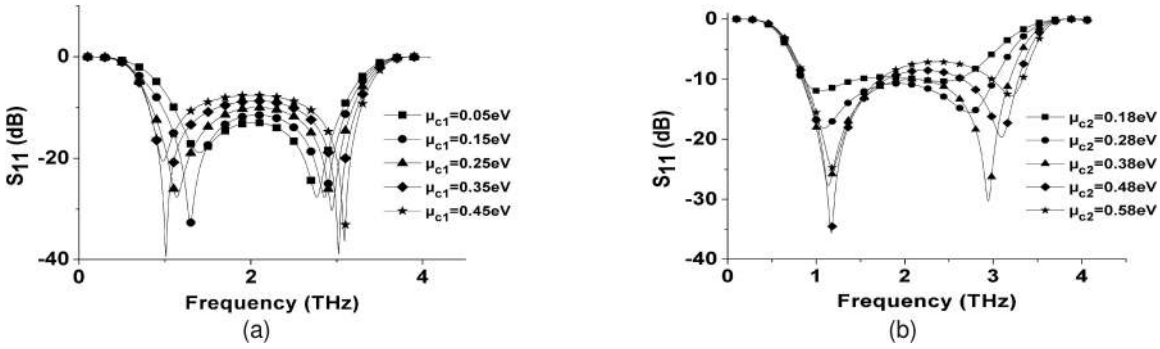

Fig. 6. Effect of graphene chemical potential over the absorption capability of an optimal THz-MMA, i.e., GTWA-III, in the range of 0.1 to 4.0 THz. (a) Effect of μ_{c1} over RC characteristics, while keeping $\mu_{c2} = 0.25$ eV. (b) Effect of μ_{c2} over RC characteristics, while keeping $\mu_{c1} = 0.38$ eV.

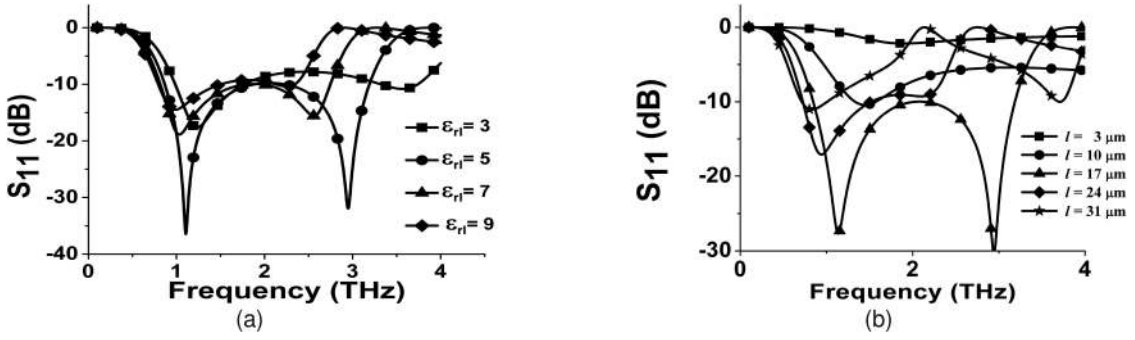

Fig. 7. Effect of the substrate design parameters over RC characteristics. (a). *'ϵ_{rl}'* ranging from 3 to 9, and (b) *'l'* ranging from 3 to 31 μm.

regime, when increasing μ_{c1}. In case of μ_{c2}, both the peak RC values are shifting towards the higher frequency regime. The results confirm that a proper variation in μ_c of the graphene can be utilized in an efficient design of the tunable absorber. It is noticed that the optimal values are obtained for the THz-MMA with μ_c of 0.38 eV (μ_{c1}), and 0.25 eV (μ_{c2}). The effect of substrate design parameters (i.e., substrate dielectric constant 'ϵ_{rl}' and thickness 'l') over the THz absorption characteristics of the device is carried out in the range of 0.1 to 4.0 THz. Fig. 7(a) depicts the effect of 'ϵ_{rl}' in absorption bandwidth of the optimal device. The value of 'ϵ_{rl}' is varied from 3 to 9 with a step size of 2. It can be analyzed that the absorption bandwidth first increases, and achieve maximum value at a certain value, and then decreases with the increment of 'ϵ_{rl}' up to 5. The THz absorption properties are found to be greatly influenced by the substrate thickness 'l', which is varied from 3 to 31 μm with step size of 7 μm, as shown in Fig. 7(b). The broadband THz absorption properties are observed for the device with an optimal value of 'l' as 17 μm.

The absorption bandwidth increases when 'P' increases, and achieves the maximum value at 10 μm and then decreases, as shown in Fig. 8(a). It can also be observed that the first peak RC value is shifting towards the low frequency regime with an increase in 'P'. A similar kind of effect is observed in Fig. 8(c), where the second peak RC value shifting towards the high frequency regime, with an increase in 'd'. In Fig. 8(b), the bandwidth of the device decreases, as 'g' increases. However, the best absorptivity is achieved, when 'g' approaches to 1.0 μm. Fig. 8(d) portrays the effect of 'w' on the absorption bandwidth. It is noticed that, as the value of 'w' increases, absorption bandwidth also increases. However, the optimal value of the 'w' is dependent on 'd', as it cannot exceed the half of 'd' due to geometry restrictions. It is clear that the maximum THz absorption takes place with optimal design parameters of the device, which are listed in Table 3. Further, the effect of the incident angle over the absorption characteristics is carried out. Fig. 8(e) presents the

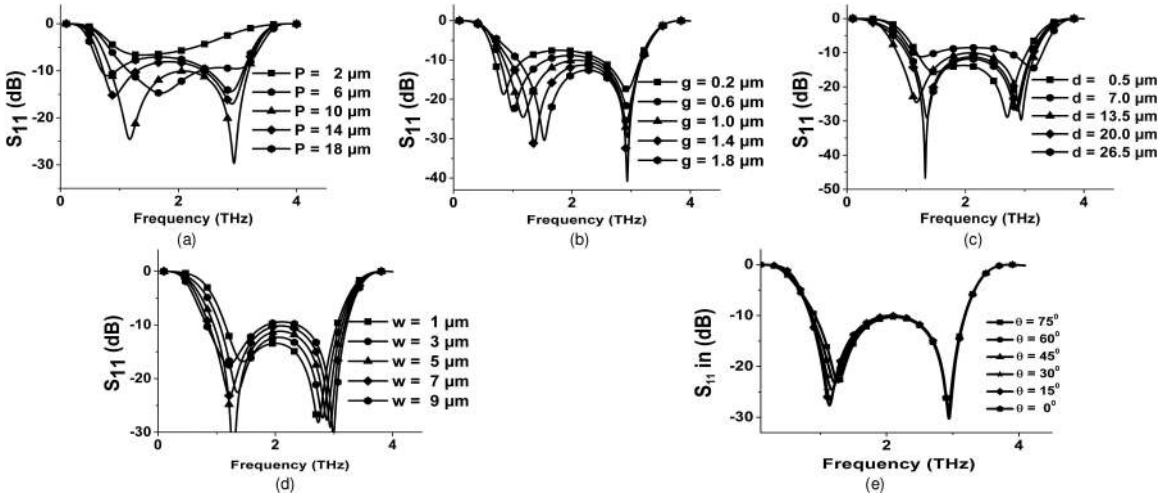

Fig. 8. Effect of FSS design variables over RC characteristics. (a) Variation in RC with patch periodicity 'P' (b) Variation in RC with patch gap 'g' (c) Variation in RC with aperture length 'd'. (d) Variation in RC with strip width 'w'. (e) Variation in RC characteristics with incident angle.

TABLE 3
Adopted THz-MMA Configurations With Corresponding Optimal Design Variables

Parameters	GTWA-I	GTWA-II	GTWA-III	GTWA-IV
μ_{c1} (FSS-I)	0.38 eV	0.70 eV	0.25 eV	0.41 eV
μ_{c2} (FSS-II)	0.25 eV	0.19 eV	0.38 eV	0.22 eV
l	23.5 μm	20 μm	17 μm	17.0 μm
t	1.0 μm	0.1 μm	0.5 μm	1.1 μm
P	10.0 μm	-	10 μm	20.0 μm
g	1.0 μm	-	1.0 μm	1.0 μm
p	-	20.1 μm	18.6 μm	20.1 μm
d	-	15.0 μm	13.5 μm	15.0 μm
w	-	5.0 μm	5.0 μm	5.0 μm

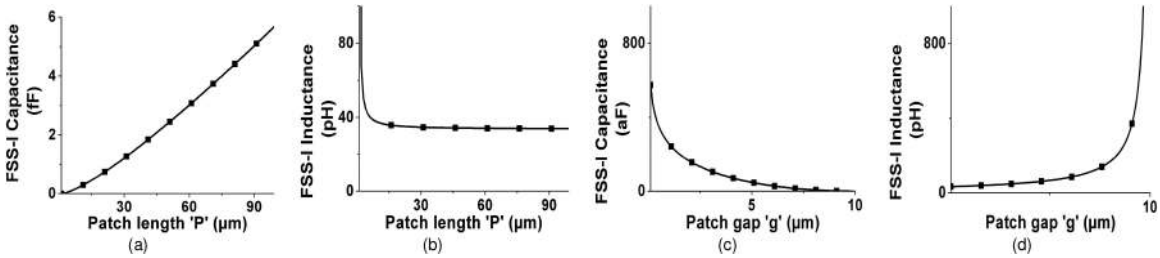

Fig. 9. Effect of design parameters of SP-FSS in its 'C_P' and 'L_P'. (a) Variation in 'C_P' w.r.t periodicity. (b) Variation in 'L_P' w.r.t periodicity. (c) Variation in 'C_P' w.r.t gap 'g'. (d) Variation in 'L_P' w.r.t gap 'g'.

variation in RC characteristics, when the incident angle varies from 0° to 75°. Clearly, no significant change in absorption bandwidth is observed, which confirms the wide incidence angle insensible (WIAI) nature of the device.

Further study is carried out to explore the physics behind the observed absorption achieved by the application graphene FSS. The absorption mechanism can be explained primarily by the impedance matching. The design parameters are optimized by ECM in the way, so that Z_{in} of the device matches with Z_o. The absorption mechanism can also be explained on the basis of circuit theory, as the variation in the device parameters leads to a corresponding variation in circuit parameters (i.e., L and C), which are responsible for the resonance at a particular frequency. Figs. 9 and 10 show

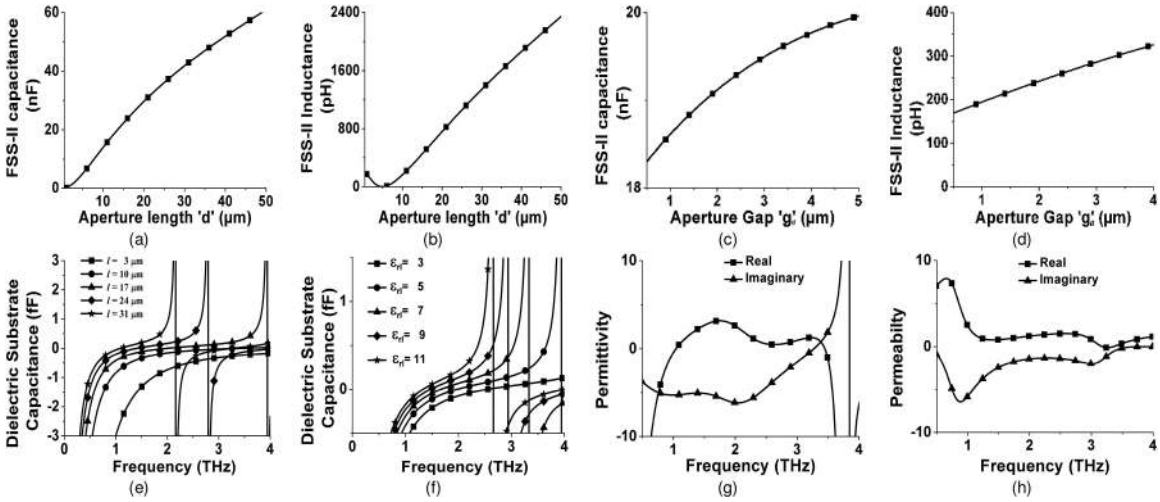

Fig. 10. Effect of design variables, (a) length of square 'd' in 'C_A' (b) length of square 'd' in 'L_A' (c) gap between two square 'g_a' in 'C_A' (d) gap between two square 'g_a' in 'L_A', and (e) substrate thickness in 'C_d', (f) dielectric constant of the substrate in 'C_d', (g) Effective permittivity (h) Effective permeability.

the dependency of the circuit parameters (i.e., L, and C) over the device design variables ('P', 'g', 'd', 'l', 'ε_{rl}' and 'g_a'). Since, the incorporation of graphene FSS is playing the major role in the achievement of broadband THz absorption, therefore, SP- FSS and SA-FSS design variables are specifically studied w.r.t. circuit parameters, as clear from Figs. 9 and 10. It can be observed that the C_p increases linearly, while L_p becomes almost constant, after a certain value of 'P', i.e., 10 μm as pictured in Figs. 9(a) and (b). On the other hand, as 'g' varies from a lower to higher value, C_p decreases, while L_p increases exponentially as figured in Figs. 9(c) and (d). However, the numerical value of C_p is very small (i.e., range of 10–15, and 10–18) as compared to the L_p (range of 10–12), which further strongly influence Z_{FSS-I}. This observation concludes that the capacitance of SP-FSS (i.e., FSS-I) is responsible for the impedance matching, and hence for the observed wideband THz wave absorption. In the case of SA-FSS, both capacitance and inductance have similar kind of variation with its design parameters as depicted in Figs. 10(a)–(d). Figs. 10(a) and (b) shows a linear variation in C_A, and L_A with a corresponding change in 'd', respectively. Similarly, in the case of 'g', both C_A, and L_A are increasing linearly, as depicted in Figs. 10(c), and (d). It can be noticed that the value of C_A is larger than the value of L_A, hence the observed absorption in this case, is primarily dominated by the inductance, instead of the capacitance. Therefore, one can say that the input impedance of SP-FSS is more influenced by the capacitance (C_P), while the input impedance of SA-FSS is governed by inductance (L_A). The parallel combination of both the FSSs (i.e., SP-FSS and SA-FSS) is governed by the lower values of the input impedance of FSS-II (i.e., SA-FSS), which is dominated by L_A. The effect of dielectric substrate parameters (i.e., 'l', and 'ϵ_{rl}') over the dielectric substrate capacitance (C_d) is presented in Figs. 10(e), and (f). It is seen that the value of C_d increases, and the resonance point shifts towards the low frequency regime, with an increment of both l and ϵ_{rl}, as depicted in Fig. 10(e), and (f), respectively. Moreover, for the optimal values of these parameters (i.e., $l = 17$ μm, and $\epsilon_{rl} = 5$), the resonance occurs at the same frequency, where the effective permittivity of the device dominates, as shown in Fig. 10(g).

THz absorption achieved by the device can also be explained on the basis of wave interference phenomena [34]. The mechanism requires the substrate thickness, sandwiched between FSS and PEC, should match with the quarter-wavelength (i.e., $\lambda/4 = 18.2$ in this case), so that the waves can cancel to each other when trapped by the absorber. The optimal dielectric substrate thickness, achieved for the device is $l = 17$ μm and thickness of polyimide layer is $t = 0.5$ μm, which make the total device thickness as 17.5 μm. This adequately satisfies the above condition for wave interference phenomena. Apart from this the induced current model, illustrated by Liao *et al.* [35], can also explain the broadband absorption. As per the research [35], the EM-coupling increases with the

TABLE 4
Comparison Between the Proposed Work and Other Reported Works

References	Structural composition	Actual thickness (μm) (Relative-thickness)	-10 dB RC bandwidth (THz)	Fractional-Bandwidth
Dong et al. [26]	FSS + SiO2 layer + Graphene stack + lightly doped Si + PEC	4.615 (0.05 λ_0)	0.98 (2.58-3.56)	31.92%
Shi et al. [27]	Heavily doped Si grating+ Si spacer	125.2 (0.67 λ_0)	1.70 (0.73-2.43)	200%
Pan et al. [29]	FSS + Dielectric layer (DL) + FSS + DL +FSS+DL+PEC	10.6 (0.04 λ_0)	0.89 (1.75-2.64)	40.64%
Wang et al. [36]	Graphene-hybrid-FSS+PMI foam+Copper floor	97.5 (0.52 λ_0)	1.34 (0.48-1.82)	116.5%
This work	Graphene-FSS+Polyimide layer+Graphene-FSS+DL+PEC	17.6 (0.24 λ_0)	2.34 (0.85-3.19)	115.84%

increase in 'l', and then decreases after an optimal value. A similar kind of pattern has been achieved in this research also, where the absorption increases, achieves maximum value, and then decreases with the increase in 'l', as shown in Fig. 7(b). Overall, it can be concluded that the combined effect of the inductance of FSSs, and capacitance of the dielectric substrate, is responsible for the broadband absorption. In order to reflect the metamaterial behavior of the device, the effective magnetic permeability, and effective dielectric permittivity of the best configuration (i.e., GTWA-III) is extracted by the methodology presented in [13]. Figs. 10(g), (h) depicts the frequency dependent spectra's of permeability. The fluctuations can be seen around the resonating frequencies (i.e., around 1.14 and 2.94 THz). Table 4 shows the comparison of proposed work with other reported works. The comparison carries out in terms of −10 dB RC bandwidth (i.e., 90% absorption bandwidth), actual thickness, and structural composition of the device. The proposed work is a simple and the optimal structure for broadband absorber with a balanced trade-off between thickness and absorption bandwidth. Clearly, it reflects the successful design of a thin and broadband THz-MMA.

4. Conclusion

In conclusion, a hybrid, tunable and thin THz absorber embedded with cascaded graphene FSS, capable of providing ultra-high broadband absorption is successfully demonstrated. The electrical properties of FSS were explored, and variation with its design parameter was analyzed. The effect of FSS design parameters and μ_c has been elucidated. In order to visualize the type of metasurface, the effective permittivity and permeability were also estimated. An optimal device is found to possess a peak RC value of −30.27 dB at 2.94 THz along with −10 dB absorption bandwidth of 2.34 THz (0.85–3.19 THz). The graphene based THz-MMA can be considered as a promising structure for emerging THz applications.

References

[1] M. Tonouchi, "Cutting-edge terahertz technology," *Nature Photon.*, vol. 1, no. 2, pp. 97–105, Feb. 2007, doi: 10.1038/nphoton.2007.3.
[2] S. W. Lee, "Scattering by dielectric-loaded screen," *IEEE Trans. Antennas Propag.*, vol. AP-19, no. 5, pp. 656–665, Sep. 1971, doi: 10.1109/TAP.1971.1140010.
[3] R. M. Woodward *et al.*, "Terahertz pulse imaging in reflection geometry of human skin cancer and skin tissue," *Phys. Med. Biol.*, vol. 47, no. 21, pp. 3853–3863, Oct. 2002, doi: 10.1088/0031-9155/47/21/325.
[4] J. Federici and L. Moeller, "Review of terahertz and subterahertz wireless communications," *J. Appl. Phys.*,vol. 107, no. 11, pp. 111101–111122, Jun. 2010, doi: 10.1063/1.3386413.
[5] D. R. Smith, J. B. Pendry, and M. C. K. Wiltshire, "Metamaterials and negative refractive index," *Science*, vol. 305, no. 5685, pp. 788–792, Aug. 2004, doi: 10.1126/science.1096796.
[6] D. R. Smith, W. J. Padilla, D. C. Vier, S. C. Nemat-Nasser, and S. Schultz, "Composite medium with simultaneously negative permeability and permittivity," *Phys. Rev. Lett.*, vol. 84, no. 18, pp. 4184–4187, May 2000, doi: 10.1103/PhysRevLett.84.4184.

[7] D. Schurig *et al.*, "Metamaterial electromagnetic cloak at microwave frequencies," *Science*, vol. 314, no. 5801, pp. 977–980, Nov. 2006, doi: 10.1126/science.1133628.

[8] H. T. Chen *et al.*, "Active terahertz metamaterial devices," *Nature*, vol. 444, no. 7119, pp. 597–600, Nov. 2006, doi: 10.1038/nature05343.

[9] T. Driscoll *et al.*, "Tuned permeability in terahertz split-ring resonators for devices and sensors," *Appl. Phys. Lett.*, vol. 91, no. 6, pp. 062511–062513, Aug. 2007, doi: 10.1063/1.2768300.

[10] N. I. Landy, S. Sajuyigbe, J. J. Mock, D. R. Smith, and W. J. Padilla, "Perfect metamaterial absorber," *Phys. Rev. Lett.*, vol. 100, no. 20, May 2008, Art. no. 207402, doi: 10.1103/PhysRevLett.100.207402.

[11] Y. Liu, S. Gu, C. Luo, and X. Zhao, "Ultra-thin broadband metamaterial absorber," *Appl. Phys. A*, vol. 108, no. 1, pp. 19–24, Jul. 2012, doi 10.1007/s00339-012-6936-0.

[12] C. Hu, Z. Zhao, X. Chen, and X. Luo, "Realizing near-perfect absorption at visible frequencies," *Opt. Exp.*, vol. 17, no. 13, pp. 11039–11044, Jun. 2009, doi: 10.1364/OE.17.011039.

[13] G. Deng, T. Xia1, J. Yang, and Z. Yin, "Triple-band polarisation-independent metamaterial absorber at mm wave frequency band," *IET Microw. Antennas Propag.*, vol. 12, no. 7, pp. 1120–1125, Jun. 2018, doi: 10.1049/iet-map.2017.0126.

[14] J. A. Mason, G. Allen, V. A. Podolskiy, and D. Wasserman, "Strong coupling of molecular and mid-infrared perfect absorber resonances," *IEEE Photon. Technol. Lett.*, vol. 24, no. 1, pp. 31–33, Jan. 2012, doi: 10.1109/LPT.2011.2171942.

[15] A. Gasmelseed and J. Yunus, "The effects of metamaterial on electromagnetic fields absorption characteristics of human eye tissues," *Prog. Biophys. Mol. Biol.*, vol. 114, no. 1, pp. 8–12, Nov. 2013, doi: 10.1016/j.pbiomolbio.2013.10.004.

[16] M. Tamagnone, J. S. Gomez-Diaz, J. R. Mosig, and J. Perruisseau-Carrier, "Reconfigurable terahertz plasmonic antenna concept using a graphene stack," *Appl. Phys. Lett.*, vol. 101, no. 21, Nov. 2012, Art. no. 214102, doi: 10.1063/1.4767338.

[17] J. S. Gomez-Diaz, J. Perruisseau-Carrier, P. Sharma, and A. Ionescu, "Non-contact characterization of graphene surface impedance at micro and millimeter waves," *J. Appl. Phys.*, vol. 111, no. 11, Jun. 2012, Art. no. 114908, doi: 10.1063/1.4728183.

[18] G. W. Hanson, "Dyadic Green's functions and guided surface waves for a surface conductivity model of graphene," *J. Appl. Phys.*, vol. 103, no. 6, Mar. 2008, Art. no. 064302, doi: 10.1063/1.2891452.

[19] V. J. Surya, K. Iyakutti, H. Mizuseki, and Y. Kawazoe, "Tuning electronic structure of graphene: A first-principle study," *IEEE Trans. Nanotechnol.*, vol. 11, no. 3, pp. 534–541, May 2012, doi: 10.1109/TNANO.2011.2182358.

[20] M. Amin, M. Farhat, and H. Baggc, "An ultra-broadband multi-layered graphene absorber," *Opt. Exp.*, vol. 21, no. 24, pp. 29938–29948, Nov. 2013, doi: 10.1364/OE.21.029938.

[21] D. Wang *et al.*, "Tunable THz multiband frequency-selective surface based on hybrid metal–graphene structures," *IEEE Trans. Nanotechnol.*, vol. 16, no. 6, pp. 1132–1137, Nov. 2017, doi: 10.1109/TNANO.2017.2749269.

[22] A. E. Yilmaz and M. Kuzuoglu, "Design of the square loop frequency selective surfaces with particle swarm optimization via the equivalent circuit model," *Radioengineering*, vol. 18, no. 2, pp. 95–102, Jun. 2009.

[23] R. Panwar and J. R. Lee, "Progress in frequency selective surface-based smart electromagnetic structures: A critical review," *Aerosp. Sci. Technol.*, vol. 66, pp. 216–234, 2017.

[24] R. Panwar and J. R. Lee, "Performance and non-destructive evaluation methods of airborne radome and stealth structures," *Meas. Sci. Technol.*, vol. 29, no. 6, Apr. 2018, Art. no. 062001, doi: 10.1088/1361-6501/aaa8aa.

[25] Y. N. Kazantsev *et al.*, "Broadening of operating frequency band of magnetic-type radio absorbers by FSS incorporation," *IEEE Trans. Antennas Propag.*, vol. 58, no. 4, pp. 1227–1235, Apr. 2010, doi: 10.1109/TAP.2010.2041316

[26] Y. Dong, P. Liu, Di. Yu, G. Li, and L. Yang, "A tunable ultrabroadband ultrathin terahertz absorber using graphene stacks," *IEEE Antennas Wireless Propag. Lett.*, vol. 16, no. 1, pp. 1115–1118, Oct. 2017, doi: 10.1109/LAWP.2016.2623316.

[27] C. Shi *et al.*, "Compact broadband terahertz perfect absorber based on multi-interference and diffraction effects," *IEEE Trans. THz Sci. Technol.*, vol. 6, no. 1, pp. 40–44, Jan. 2016, doi: 10.1109/TTHZ.2015.2496313.

[28] Y. Q. Ye, Y. Jin, and S. He, "Omnidirectional, polarization-insensitive and broadband thin absorber in the terahertz regime," *J. Opt. Soc. Amer. B*, vol. 27, no. 3, pp. 498–504, Mar. 2010, doi: 10.1364/JOSAB.27.000498.

[29] W. Pan, X. Yu, J. Zhang, and W. Zeng, "A novel design of broadband terahertz metamaterial absorber based on nested circle rings," *IEEE Photon. Technol. Lett.*, vol. 28, no. 21, pp. 2335–2338, Nov. 2016, doi: 10.1109/LPT.2016.2593699.

[30] D. S. Wilbert, M. P. Hokmabadi, P. Kung, and S. M. Kim, "Equivalent-circuit interpretation of the polarization insensitive performance of THz metamaterial absorbers," *IEEE Trans. THz Sci. Technol.*, vol. 3, no. 6, pp. 846–850, Nov. 2013, doi: 10.1109/TTHZ.2013.2285311.

[31] X. Huang, X. Zhang, Z. Hu, M. Aqeeli, and A. Alburaikan, "Design of broadband and tunable terahertz absorbers based on graphene metasurface: Equivalent circuit model approach," *IET Microw. Antennas Propag.*, vol. 9, no. 4, pp. 307–312, 2015, doi: 10.1049/iet-map.2014.0152.

[32] R. Mishra, R. Panwar, and D. Singh, "Equivalent circuit model for the design of frequency-selective, terahertz-band, graphene-based metamaterial absorbers," *IEEE Magn. Lett.*, vol. 9, Oct. 2018, Art. no. 3707205, doi: 10.1109/LMAG.2018.2878946.

[33] B. A. Munk, *Frequency Selective Surfaces: Theory and Design*. New York, NY, USA: Wiley, 2000, pp. 365–375, doi: 10.1002/0471723770.

[34] M. Kenney, J. Grant, Y. D. Shah, I. Escorcia-Carranza, M. Humphreys, and D. R. S. Cumming, "Octave-spanning broadband absorption of terahertz light using metasurface fractal-cross absorbers," *ACS Photon.*, vol. 4, pp. 2604–2612, Sep. 2017, doi: 10.1021/acsphotonics.7b00906.

[35] Z. Liao, R. Gong, Y. Nie, T. Wang, and X. Wang, "Absorption enhancement of fractal frequency selective surface absorbers by using microwave absorbing material based substrates," *Photon. Nanostruct. – Fundam. Appl.*, vol. 9, no. 3, pp. 287–294, Jul. 2011, doi: 10.1016/j.photonics.2011.05.006.

[36] L. Wang *et al.*, "An ultra-broadband THz absorber based on graphene," presented at the *11th Int. Symp. Antennas, Propag.*, EM Theory, Guilin, China, Oct. 18–21, 2016.